Transversely Isotropic Plasticity with Application to Fiber-Reinforced Plastics

M. Vogler[1], S. Kolling[2], R. Rolfes[1]

[1] Leibniz University Hannover, Institute for Structural Analysis, 30167 Hannover
[2] DaimlerChrysler AG, EP/SPB, HPC X271, 71059 Sindelfingen

Abstract:

In this article a constitutive formulation for transversely isotropic materials is presented taking large plastic deformation at small elastic strains into account. A scalar damage model is used for the approximation of the unloading behavior. Furthermore, a failure surface is assumed taking the influence of triaxiality on fracture into account. Regularization is considered by the introduction of an internal length for the computation of the fracture energy. The present formulation is applied to the simulation of tensile tests for a molded glass fibre reinforced polyurethane material.

Keywords:

Anisotropy, Transversely Isotropy, Structural Tensors, Plasticity, Anisotropic Damage, Failure, Fiber Reinforced Plastics

1 Introduction

Most of the materials that are used in the automotive industry are anisotropic to some degree. This material behavior can be observed in metals as well as in non-metallic materials like molded components of fibre reinforced plastics among others.
In metals, the anisotropy is induced during the manufacturing process, e.g. during sheet metal forming and due to direction of rolling. In fibre-reinforced plastics, the anisotropy is determined by the direction of the fibres.

The state-of-the-art in the numerical simulation of structural parts made from fibre reinforced plastics represents GLASER's model [1]. In this visco-plastic formulation, fibre orientations are obtained from a moldflow-analysis. This information is then used locally in each GAUSS-point where a homogenization procedure yields the overall properties. In particular, this formulation has its advantage for fibre reinforced thermoplastics where the fibre orientations change along the thickness of a structural part, i.e. flow aligned at the boundaries and perpendicular aligned in the middle.

An alternative approach is presented by KRIVACHY [2] using a material model with orthotropic elasticity and orthotropic visco-plasticity. Test specimens in and perpendicular to the flow direction are taken from a molded plate to produce the required input data. The yield surface in this model is chosen as proposed by JUNGINGER [3].

In this article, a constitutive model for transversely isotropic materials is presented. The formulation takes the following features into account:

- large plastic deformation at small elastic strains
- C^1-continuous yield surface
- scalar damage for the approximation of the unloading behavior
- anisotropic damage evolution
- general failure surface considering triaxiality
- regularization and fracture energy

The main focus is set on glass fibre reinforced polyurethane molded products that find their applications in front/rear ends and fenders among others. For this class of materials, the fibre orientation is more or less constant along the thickness of the structural part. The required input data may thus be obtained by tensile tests with specimens taken from a molded plate in flow direction and perpendicular to it. The validation and verification of this test data shows the practicability of the chosen approach.

2 Constitutive Model

Transversely isotropic materials are characterized by a preferred direction $\mathbf{a}$. Thus, the material response is invariant with respect to arbitrary rotations around this preferred

direction $\mathbf{a}$, to reflections at fiber parallel planes and with respect to the reflection at that plane, whose normal is $\mathbf{a}$. These are the group of symmetry transformations for transverse isotropy. The structural tensor $\mathbf{A}$ of transverse isotropy, which represents the material's intrinsic characteristic, is defined as the dyadic product of the preferred direction $\mathbf{a}$

$$\mathbf{A} = \mathbf{a} \otimes \mathbf{a} \quad . \tag{1}$$

As the elastic range of the material is assumed to be small, an additive decomposition of the strain tensor is justified:

$$\boldsymbol{\varepsilon} = \boldsymbol{\varepsilon}^e + \boldsymbol{\varepsilon}^p \quad . \tag{2}$$

In the subsequent representations, isotropic tensor functions for the elastic free energy and the yield surface are derived.

2.1 Elastic Stress Strain Relations

Considering only small elastic deformations, HOOKE's linear elasticity law $\boldsymbol{\sigma} = \hat{\boldsymbol{\sigma}}(\boldsymbol{\varepsilon}) = \mathbb{C}_e \boldsymbol{\varepsilon}$ is assumed. Postulating hyperelasticity, the first derivative of the free energy function $\hat{\Psi}$ with respect to the strains $\boldsymbol{\varepsilon}$ yields the stresses $\boldsymbol{\sigma}$ and the second derivation with respect to the strains $\boldsymbol{\varepsilon}$ gives the elasticity tensor $\mathbb{C}_e$. In case of transverse isotropy, the free energy function is formulated in isotropic invariants of the strain tensor $\boldsymbol{\varepsilon}$ and the structural tensor $\mathbf{A}$, see [5]. To derive a representation of $\hat{\Psi}$ and the infinitesimal stress tensor $\boldsymbol{\sigma}$ as isotropic tensor-functions, the functional basis of the two symmetric second order tensorial arguments $\boldsymbol{\sigma}$ and $\mathbf{A}$ is needed. Assuming the stresses to be a linear function of the strains and providing a stress free undistorted initial configuration, i.e. $\boldsymbol{\sigma}(\boldsymbol{\varepsilon} = 0) = 0$, such terms are neglected, which are linear or cubic in the strains. This enforces the elasticity tensor $\mathbb{C}_e$ to be constant and yields to a formulation of the free energy function with five elasticity constants λ, α, μ_L, μ_T and β describing the transversely isotropic material behavior:

$$\begin{aligned} \hat{\Psi}(\boldsymbol{\varepsilon}, \mathbf{A}) := \; & \frac{1}{2}\lambda(\operatorname{tr}\boldsymbol{\varepsilon})^2 + \mu_T \operatorname{tr}(\boldsymbol{\varepsilon})^2 + \alpha(\mathbf{a}^T\boldsymbol{\varepsilon}\mathbf{a}) \operatorname{tr}\boldsymbol{\varepsilon} + \\ & 2(\mu_L - \mu_T)(\mathbf{a}^T\boldsymbol{\varepsilon}^2\mathbf{a}) + \frac{1}{2}\beta(\mathbf{a}^T\boldsymbol{\varepsilon}\mathbf{a})^2 \quad . \end{aligned} \tag{3}$$

For the stresses we obtain

$$\begin{aligned} \boldsymbol{\sigma} = \; & \lambda(\operatorname{tr}\boldsymbol{\varepsilon})\mathbf{1} + 2\mu_T\boldsymbol{\varepsilon} + \alpha(\mathbf{a}^T\boldsymbol{\varepsilon}\mathbf{a}\,\mathbf{1} + \operatorname{tr}\boldsymbol{\varepsilon}\,\mathbf{A}) \\ & + 2(\mu_L - \mu_T)(\mathbf{A}\boldsymbol{\varepsilon} + \boldsymbol{\varepsilon}\mathbf{A}) + \beta\left(\mathbf{a}^T\boldsymbol{\varepsilon}\mathbf{a}\right)\mathbf{A} \end{aligned} \tag{4}$$

and the elasticity tensor is written as

$$\begin{aligned} \mathbb{C}_e = \; & \lambda\mathbf{1}\otimes\mathbf{1} + 2\mu_T\mathbb{I} + \alpha(\mathbf{A}\otimes\mathbf{1} + \mathbf{1}\otimes\mathbf{A}) \\ & + 2(\mu_L - \mu_T)\mathbb{I}_{\mathbf{A}} + \beta\mathbf{A}\otimes\mathbf{A} \quad . \end{aligned} \tag{5}$$

Hereby, the 4th order tensor $\mathbb{I}_{\mathbf{A}}$ in index notation reads $A_{im}\mathbb{I}_{jmkl} + A_{jm}\mathbb{I}_{mikl}$. In matrix notation the 4th order elasticity tensor of transversely isotropic material for a preferred X_1-direction in a Cartesian coordinate system, i.e. $\mathbf{a} = [1, 0, 0]^T$, reads:

$$\mathbb{C}_e = \begin{bmatrix} \lambda + 2\alpha + \beta + 4\mu_L - 2\mu_T & \lambda + \alpha & \lambda + \alpha & 0 & 0 & 0 \\ \lambda + \alpha & \lambda + 2\mu_T & \lambda & 0 & 0 & 0 \\ \lambda + \alpha & \lambda & \lambda + 2\mu_T & 0 & 0 & 0 \\ 0 & 0 & 0 & \mu_L & 0 & 0 \\ 0 & 0 & 0 & 0 & \mu_L & 0 \\ 0 & 0 & 0 & 0 & 0 & \mu_T \end{bmatrix} . \tag{6}$$

The transformation from engineering constants to those of the invariant representation and vice versa are listed in tab. 1.

- symmetry of the elasticity tensor:
  $\frac{\nu_{12}}{E_{22}} = \frac{\nu_{21}}{E_{11}}; \quad \frac{\nu_{13}}{E_{33}} = \frac{\nu_{31}}{E_{11}}; \quad \frac{\nu_{23}}{E_{33}} = \frac{\nu_{32}}{E_{22}}$
- constants of invariant formulation:
  $\lambda = E_{22}(\nu_{23} + \nu_{31}\nu_{13})/D$
  $\alpha = E_{22}[\nu_{31}(1 + \nu_{32} - \nu_{13}) - \nu_{32}]/D$
  $\beta = E_{11}(1 - \nu_{32}\nu_{23})/D - E_{22}[\nu_{23} + \nu_{13}\nu_{31}]/D - 4\mu_{12}$
  $\mu_l = \mu_{12}$
  $\mu_t = \mu_{23}$
  $D = 1 - \nu_{32}^2 - 2\nu_{13}\nu_{31} - 2\nu_{32}\nu_{31}\nu_{13}$
- engineering constants:
  $E_{22} = E_{33}, \quad \nu_{23} = \nu_{32}, \quad \nu_{12} = \nu_{13}, \quad \nu_{21} = \nu_{31}, \quad \mu_{12} = \mu_{13}$
  $E_{11} = -(\lambda\mu_t - 4\lambda\mu_l - \lambda\beta - 2\alpha\mu_t + 2\mu_t^2 - \beta\mu_t - 2\alpha\mu_t - 4\mu_l\mu_t + \alpha^2)/(\lambda + \mu_t)$
  $E_{22} = -4\mu_t(\lambda\mu_t - 4\mu_l\lambda - \beta\lambda + 2\mu_t^2 - \beta\mu_t - 2\alpha\mu_t - 4\mu_t\mu_l + \alpha^2)/D_t$
  $\nu_{12} = 2\mu_t(\lambda + \alpha)/D_t$
  $\nu_{21} = (\lambda + \alpha)/(2\lambda + 2\mu_t)$
  $\nu_{23} = -(\alpha^2 + 2\lambda\mu_t - \beta\lambda - 4\mu_l\lambda)/D_t$
  $\mu_{12} = \mu_l$
  $\mu_{23} = \mu_t$
  $D_t = 4\mu_l\lambda + \beta\lambda - 4\mu_t^2 + 4\mu_t\alpha + 2\beta\mu_t + 8\mu_l\mu_t - \alpha^2$

Table 1: elasticity constants for transversely isotropic elasticity

2.2 Transversely Isotropic Yield Surface

Our proposal of a transversely isotropic yield surface is an extension of a yield function following [21] and [20] and its numerical treatment in [17] and [22]. This model is based on two assumptions, on plastic incompressibility and that projections of stresses onto the preferred direction $\mathbf{a}$ do not induce plastic yielding. This condition is taken into account

by a decomposition of the stress tensor into an extra stress tensor $\boldsymbol{\sigma}^{\text{pind}}$, inducing plastic yielding, and a remaining reaction stress tensor $\boldsymbol{\sigma}^{\text{reac}}$:

$$\boldsymbol{\sigma} = \boldsymbol{\sigma}^{\text{pind}} + \boldsymbol{\sigma}^{\text{reac}} \quad . \tag{7}$$

The assumption of plastic incompressibility is fulfilled with the postulation

$$\text{tr}\,\boldsymbol{\sigma}^{\text{pind}} = 0 \quad . \tag{8}$$

Presuming inextensibility of the preferred direction $\mathbf{a}$, in which plasticity is assumed not to occur, leads to an additional constraint. The projection of the stress tensor onto the fiber direction $\mathbf{a}$ must vanish:

$$\mathbf{a}\boldsymbol{\sigma}^{\text{pind}}\mathbf{a} = \underbrace{\mathbf{a}\otimes\mathbf{a}}_{:=\,\mathbf{A}} : \boldsymbol{\sigma}^{\text{pind}} = 0 \quad . \tag{9}$$

$\mathbf{A}$ is the structural tensor belonging to the fiber direction $\mathbf{a}$. With eq. (8), eq. (9) and an ansatz for $\boldsymbol{\sigma}^{\text{reac}}$ of the form

$$\boldsymbol{\sigma}^{\text{reac}} = p\mathbf{1} + T_a\,\mathbf{A} \quad , \tag{10}$$

the stress components $\boldsymbol{\sigma}^{\text{reac}}$ and $\boldsymbol{\sigma}^{\text{pind}}$ yield

$$\begin{aligned} \boldsymbol{\sigma}^{\text{reac}} &= \underbrace{\frac{1}{2}(\,\text{tr}\,\boldsymbol{\sigma} - \mathbf{a}\boldsymbol{\sigma}\mathbf{a})}_{p}\,\mathbf{1} \underbrace{-\frac{1}{2}(\,\text{tr}\,\boldsymbol{\sigma} - 3\mathbf{a}\boldsymbol{\sigma}\mathbf{a})}_{T_a}\,\mathbf{A} \\ \boldsymbol{\sigma}^{\text{pind}} &= \boldsymbol{\sigma} - \frac{1}{2}(\,\text{tr}\,\boldsymbol{\sigma} - \mathbf{a}\boldsymbol{\sigma}\mathbf{a})\mathbf{1} + \frac{1}{2}(\,\text{tr}\,\boldsymbol{\sigma} - 3\mathbf{a}\boldsymbol{\sigma}\mathbf{a})\mathbf{A} \quad . \end{aligned} \tag{11}$$

As can be seen in the following equation, T_a can be interpreted as a fiber overstress, exceeding the hydrostatical part of the stress tensor. The total stress of the fiber is

$$\mathbf{a}^T\boldsymbol{\sigma}\mathbf{a} = \mathbf{a}^T\boldsymbol{\sigma}^{\text{reac}}\mathbf{a} = p + T_a \quad . \tag{12}$$

To account for an influence of plastification in fiber direction, the projection of the deviatoric part of the reaction stress tensor $\boldsymbol{\sigma}^{\text{reac}}$ onto $\mathbf{a}$ can be regarded:

$$\mathbf{a}^T(\,\text{dev}\,\boldsymbol{\sigma}^{\text{reac}})\mathbf{a} = \mathbf{a}^T\,T_a(\,\text{dev}\,\mathbf{A})\mathbf{a} = T_a\,\mathbf{a}^T(\mathbf{A} - \frac{1}{3}\mathbf{1})\mathbf{a} = \frac{2}{3}T_a \quad . \tag{13}$$

The construction of the anisotropic yield condition follows the same considerations as the derivation of the hyperelastic potential $\hat{\Psi}$. The yield function has to be invariant with respect to transformations belonging to the group of symmetry transformations for transverse isotropy. The yield condition can be composed of the basic invariants of the related stresses and the structural tensor. The invariants I_1 and I_2 are formulated with $\boldsymbol{\sigma}^{\text{pind}}$, following a proposal of Schröder [17], who refers to the work of Spencer [20] and Rogers [21]:

$$\begin{aligned} I_1 &:= \frac{1}{2}\,\text{tr}\,(\boldsymbol{\sigma}^{\text{pind}})^2 - \mathbf{a}^T\,(\boldsymbol{\sigma}^{\text{pind}})^2\,\mathbf{a} \quad , \\ I_2 &:= \mathbf{a}^T\,(\boldsymbol{\sigma}^{\text{pind}})^2\,\mathbf{a} \quad . \end{aligned} \tag{14}$$

If only these two invariants are considered in the yield locus, solely shear deformations are assumed to cause plastic yielding. If yielding in the preferred fiber direction should be considered, an additional invariant, formulated in deviatoric stresses, is introduced:

$$I_4 := \frac{3}{2}\mathbf{a}^T\boldsymbol{\sigma}^{\mathrm{dev}}\mathbf{a} = T_a \quad . \tag{15}$$

In order to account for a pressure dependency of the yield locus, a further invariant, representing the hydrostatical pressure is introduced:

$$I_3 := \ \mathrm{tr}\,\boldsymbol{\sigma} - \mathbf{a}^T\boldsymbol{\sigma}\mathbf{a} \quad . \tag{16}$$

The yield function as a function of the introduced invariants is formulated as

$$f = \alpha_1\, I_1 + \alpha_2\, I_2 + \alpha_3 I_3 + \alpha_{32} I_3^2 + \alpha_4\, I_4^2 - 1 \tag{17}$$

with the flow parameters α_1, α_2, α_3, α_{32} and α_4. The derivations of the yield surface are:

$$\begin{aligned} \partial_{\boldsymbol{\sigma}} f &= \partial_{I_i} f\ \partial_{\boldsymbol{\sigma}} I_i f = \\ &\quad \alpha_1\,\boldsymbol{\sigma}^{\mathrm{pind}} + (\alpha_2 - \alpha_1)\,(\mathbf{A}\,\boldsymbol{\sigma}^{\mathrm{pind}} + \boldsymbol{\sigma}^{\mathrm{pind}}\mathbf{A}) + \alpha_3(\mathbf{1} - \mathbf{A}) \\ &\quad +2\alpha_{32} I_3(\mathbf{1} - \mathbf{A})\alpha_4\,(3\,I_4\mathbf{A}^{\mathrm{dev}}) \ =: \ \mathbb{A} : \boldsymbol{\sigma} + \mathbf{B} \\ \partial^2_{\boldsymbol{\sigma}\boldsymbol{\sigma}} f &= \alpha_1\,\mathbb{P}^{\mathrm{pind}} + (\alpha_2 - \alpha_1)\,\mathbb{P}^{\mathrm{pind}}_{\mathbf{A}} + 2\alpha_{32}(\mathbf{1} - \mathbf{A}) \otimes (\mathbf{1} - \mathbf{A}) \\ &\quad +\alpha_3(\mathbf{1} - \mathbf{A})\frac{9}{2}\,\alpha_4\,\mathbf{A}^{\mathrm{dev}} \otimes \mathbf{A}^{\mathrm{dev}} \ =: \ \mathbb{A} \end{aligned} \tag{18}$$

with the projection tensor

$$\mathbb{P}^{\mathrm{pind}} := \partial_{\boldsymbol{\sigma}}\boldsymbol{\sigma}^{\mathrm{pind}} = \mathbb{I} - \frac{1}{2}(\mathbf{1} \otimes \mathbf{1}) + \frac{1}{2}(\mathbf{A} \otimes \mathbf{1} + \mathbf{1} \otimes \mathbf{A}) - \frac{3}{2}(\mathbf{A} \otimes \mathbf{A}) \tag{19}$$

and $(\mathbb{P}^{\mathrm{pind}}_{\mathbf{A}})_{ijkl} := A_{im}\mathbb{P}^{\mathrm{pind}}_{mjkl} + A_{mj}\mathbb{P}^{\mathrm{pind}}_{imkl}$.

$\mathbf{A}^{\mathrm{dev}}$ is the deviator of the structural tensor $\mathbf{A}$, $\mathbb{A}$ is the constant bending tensor and $\mathbf{B}$ is the first derivative of the linear terms in $\boldsymbol{\sigma}$ of the quadratic yield locus. This enables us to state the yield function eq. (17) in the more general form

$$f = \frac{1}{2}\boldsymbol{\sigma} : \mathbb{A} : \boldsymbol{\sigma} + \mathbf{B} : \boldsymbol{\sigma} - 1 \quad . \tag{20}$$

2.3 Hardening Formulation

In the present material law, an isotropic hardening model is implemented. In analogy to the material model SAMP-1 [4], the hardening formulation is fully tabulated and consequently the user can directly input measurement results from material testings in terms of load curves giving the yield stress as a function of the corresponding plastic strain. Thus, test results that are reflected in the load curves will be used exactly in the simulation without time consuming parameter fitting. The tabulated input of hardening curves requires true stresses over true plastic strains. As the hardening curves usually are measured as stresses over total strains, the curves has to be prepared by subtracting the elastic part of the strains from the total strains. If hardening data are given as engineering stresses and engineering strains, a conversion into true stresses and true strains has to be performed, see also [4] for further description.

2.3.1 Parameter Identification

In order to determine the five material parameters α_1, α_2, α_3, α_{32} and α_4 of the yield function (17), five material tests are required, giving the yield stresses over the plastic strains. Concerning the numerical treatment, a table lookup is performed in every time step and the yield surface parameters are updated. As input serve the corresponding plastic strain for each material test. In the sequel, the conversion of the yield stresses y into the yield surface parameters are derived. The chosen material tests should be understood as an example of a possible set of tests. Of course, any of these testings can be replaced by other suitable material tests if available. The following five material tests are suggested to determine the yield surface parameters :

1. tension in fiber direction

$$\boldsymbol{\sigma} = \operatorname{dev}\boldsymbol{\sigma} = \begin{bmatrix} y_a & 0 & 0 \\ 0 & 0 & 0 \\ 0 & 0 & 0 \end{bmatrix}, \qquad \mathbf{a} = \begin{bmatrix} 1 \\ 0 \\ 0 \end{bmatrix}, \qquad \boldsymbol{\sigma}^{\text{pind}} = \mathbf{0}$$

$$I_1 = 0\,, \qquad I_2 = 0\,, \qquad I_4 = y_a$$

$$\rightsquigarrow \qquad f = \alpha_4 I_4^2 - 1 = 0$$

$$\boxed{\alpha_4 := 1/y_a^2} \tag{21}$$

2. simple shear in the plane perpendicular to the fiber (transverse shear)

$$\boldsymbol{\sigma} = \operatorname{dev}\boldsymbol{\sigma} = \boldsymbol{\sigma}^{\text{pind}} = \begin{bmatrix} 0 & y_{tr} & 0 \\ y_{tr} & 0 & 0 \\ 0 & 0 & 0 \end{bmatrix}, \qquad \mathbf{a} = \begin{bmatrix} 0 \\ 0 \\ 1 \end{bmatrix}$$

$$I_1 = y_{tr}^2\,, \qquad I_2 = 0\,, \qquad I_3 = 0\,, \qquad I_4 = 0$$

$$\rightsquigarrow \qquad f = \alpha_1 y_{tr}^2 - 1 = 0$$

$$\boxed{\alpha_1 := 1/y_{tr}^2} \tag{22}$$

3. simple shear in the fiber plane (in-plane shear)

$$\boldsymbol{\sigma} = \operatorname{dev}\boldsymbol{\sigma} = \boldsymbol{\sigma}^{\text{pind}} = \begin{bmatrix} 0 & y_{ip} & 0 \\ y_{ip} & 0 & 0 \\ 0 & 0 & 0 \end{bmatrix}, \qquad \mathbf{a} = \begin{bmatrix} 1 \\ 0 \\ 0 \end{bmatrix}$$

$$I_1 = 0\,, \qquad I_2 = y_{ip}^2\,, \qquad I_3 = 0\,, \qquad I_4 = 0$$

$$\rightsquigarrow \qquad f = \alpha_2 y_{ip}^2 - 1 = 0$$

$$\boxed{\alpha_2 := 1/y_{ip}^2} \tag{23}$$

4. uniaxial tension and uniaxial compression perpendicular to the fiber

$$\boldsymbol{\sigma} = \begin{bmatrix} 0 & 0 & 0 \\ 0 & 0 & 0 \\ 0 & 0 & y_{uni} \end{bmatrix}, \qquad \mathbf{a} = \begin{bmatrix} 1 \\ 0 \\ 0 \end{bmatrix}$$

$$I_1 = \frac{y_{uni}^2}{4}, \qquad I_2 = 0, \qquad I_3 = y_{uni}, \qquad I_4 = 0$$

$$\rightsquigarrow \qquad f = \alpha_1 \frac{y_{uni}^2}{4} + \alpha_3 y_{uni} + \alpha_{23} (y_{uni})^2 - 1 = 0$$

The parameter α_1 is known from the second material test (transverse shear), so two parameters α_3 and α_{32} remain to be determined. Inserting in the yield function for y_{uni}, the yield stresses from uniaxial tension y_{ut} and uniaxial compression y_{uc} leads to a system of equations with two equations and two unknowns from which the parameters α_3 and α_{32} can be obtained:

$$\boxed{\alpha_{32} := \frac{\dfrac{1}{y_{ut}} - \dfrac{1}{y_{uc}} - \dfrac{\alpha_1}{4}(y_{ut} - y_{uc})}{y_{ut} - y_{uc}}} \tag{24}$$

$$\boxed{\alpha_3 := \frac{1}{y_{ut}} - \frac{\alpha_1}{4} y_{ut} - \alpha_{32} y_{ut}} \tag{25}$$

A typical material test, which is often delivered with material data, is a tensile test in direction of 45° to the fibers. This material test can replace a test contained in the suggested set of material tests to obtain the yield surface parameters.

- tension 45° to fiber direction

$$\boldsymbol{\sigma} = \begin{bmatrix} y_a & 0 & 0 \\ 0 & 0 & 0 \\ 0 & 0 & 0 \end{bmatrix}, \qquad \mathbf{a} = \begin{bmatrix} 0.7071 \\ 0.7071 \\ 0 \end{bmatrix}$$

$$I_1 = \frac{y_{uni}^2}{16}, \qquad I_2 = \frac{y_{uni}^2}{4}, \qquad I_3 = \frac{y_{uni}}{2} \qquad I_4 = \frac{y_{uni}}{4}$$

$$\rightsquigarrow \qquad f = \alpha_1 I_1 + \alpha_2 I_2 + \alpha_3 I_3 + \alpha_{32} I_3^2 + \alpha_4 I_4^2 - 1$$

2.4 Damage

Some application in engineering practice require simulation of the unloading behavior of a material. E.g. for leg impact simulations, the approximation of the viscous unloading behavior is of major importance, see [12] and [8]. This behavior can be approximated linearly by a scalar damage approach decreasing the elastic material properties. In the present material model, a transversely isotropic damage model is implemented. It is assumed that

damage in the preferred direction and transverse evolves differently. Therefore, two scalar damage parameters $d_\perp$ and $d_\parallel$ are introduced. The implemented damage model uses the notion of effective cross section, which is the true cross section of the material minus the cracks that have developed:

$$A_{eff} = A(1-d) \quad . \tag{26}$$

This allows the definition of an effective stress

$$\sigma_{eff} = \frac{F}{A_{eff}} = \frac{F}{A(1-d)} = \frac{\sigma}{1-d} \, , \tag{27}$$

see [9]. Accordingly, the effective yield stress is given by

$$\sigma_{y,eff} = \frac{\sigma_y}{(1-d)} \quad . \tag{28}$$

By application of the principle of strain equivalence, stating that if the undamaged modulus is used, the effective stress corresponds to the same elastic strain as the true stress using the damaged modulus, one can write:

$$E = \frac{\sigma_{eff}}{\varepsilon_{el}} \quad , \tag{29}$$

$$E_d = \frac{\sigma}{\varepsilon_{el}} = E(1-d) \quad . \tag{30}$$

In order to determine the damage parameters $d_\perp$ and $d_\parallel$, unloading tests at different strain levels both in fiber direction and transverse has to be performed. The unloading curves can be approximated with a straight line, giving the damaged elastic modules $E_{\parallel,d}$ and $E_{\perp,d}$ in dependence of the accumulated uniaxial plastic strains $\varepsilon^p_\parallel$ and $\varepsilon^p_\perp$ respectively. The damage variables $d_\perp$ and $d_\parallel$ are calculated with eq. (32).

$$d(\varepsilon^p_\parallel) = 1 - \frac{E_{\parallel,d}}{E_\parallel} \quad , \tag{31}$$

$$d(\varepsilon^p_\perp) = 1 - \frac{E_{\perp,d}}{E_\parallel} \quad . \tag{32}$$

These experimentally measured damage parameters are required as tabulated data for the material model. The plastic strains in the preferred direction and transverse are

$$\varepsilon^p_\parallel = \mathbf{a}^T \, \boldsymbol{\varepsilon}^{p\,\mathrm{dev}} \, \mathbf{a} \quad , \tag{33}$$

$$\varepsilon^p_\perp = \sqrt{\frac{2}{3} \left(\boldsymbol{\varepsilon}^{p\,\mathrm{dev}} - \varepsilon^p_\parallel \mathbf{A} \right) : \left(\boldsymbol{\varepsilon}^{p\,\mathrm{dev}} - \varepsilon^p_\parallel \, \mathbf{A} \right)} \quad . \tag{34}$$

In this case, the numerically computed stress values will correspond to the input data and the damage model will seem to affect only the elastic modulae and thus the unloading and reloading behavior of the material.

2.5 Failure

Whereas the damage formulation in sec. 2.4 only affects the elastic material properties, this section is concerned with material softening with subsequent material failure after a certain critical stress state is exceeded. Therefore, two damage initiation criterions are introduced. The first one, the fiber failure criterion, only accounts for the stress resistance in fiber direction, whereas the second one, the inter-fiber failure criterion, regards stress states caused by shear stresses and loadings perpendicular to the fiber direction. However, if the inter-fiber criterion is active, the stresses in fiber direction are not effected, whereas, if the fiber failure criterion is achieved, the material collapses and the affected elements are removed from the mesh.

2.5.1 Fiber Failure Criterion

It is assumed, that the strength in fiber direction is mainly governed by the strength of the fibers. Thus, in the material model a fiber tensile strength $R_{\parallel}^{t}$ and a compressive strength $R_{\parallel}^{c}$, representing the resistance of the fiber bundle under uniaxial tension and compression in fiber direction, are needed as input data. Theses ultimate stresses are obtained from experiment. If one of these strengths is achieved, the material fails and there is no remaining load carrying capacity. The failure criterion for fiber failure is :

$$F_{ff} = \frac{\mathbf{a}^T \boldsymbol{\sigma} \mathbf{a}}{R_{\parallel}} = 1 \quad . \tag{35}$$

The term $\mathbf{a}^T \boldsymbol{\sigma} \mathbf{a}$ is the projection of the stress tensor onto the preferred direction and $R_{\parallel}$ is the resistance of the fiber bundle in fiber direction in tension ($R_{\parallel} = R_{\parallel}^{t}$) and in compression ($R_{\parallel} = R_{\parallel}^{c}$) respectively. If the fiber failure criterion is active, a scalar damage variable d_{ff} is set and stiffness degradation governed by fracture energy formulation of HILLERBORG is applied, see [18]. The stiffness degradation caused by damage parameter d_{ff} effects all stresses in any direction.

$$\boldsymbol{\sigma}_{dam} = (1 - d_{ff})\, \boldsymbol{\sigma}_{eff} \ , \tag{36}$$

2.5.2 Inter-Fiber Failure Criterion

To consider stress states out of the fiber direction, a further damage criterion is introduced. This inter-fiber failure criterion is formulated similar to the yield locus in the $\sqrt{I_1}$-I_3-invariant-plane, as illustrated in fig. 1. The failure surface is given by

$$F_{iff} = \beta_1 I_1 + \beta_2 I_2 + \beta_3 I_3 + \beta_{32} I_3^2 = 1 \quad . \tag{37}$$

The failure criterion is active, when $F_{iff} = 1$. The parameters β_1, β_3 and β_{32} are obtained in the same manner as the parameters α_1, α_2, α_3 and α_{32} for the yield function eq. (17). Therefore, the material strengths of uniaxial tension $R_{\perp}^{t}$ and compression $R_{\perp}^{c}$ perpendicular to the fiber and the material strength of transverse shear $R_{\perp\perp}$ and in-plane shear

$R_{\parallel\perp}$ has to be inserted instead of the yield stresses in eq. (17). The required strengths $R^t_\perp$, $R^c_\perp$, $R_{\perp\perp}$ and $R_{\parallel\perp}$ are obtained from material tests.

$$\begin{aligned}
\beta_1 &:= 1/R^2_{\perp\perp} \quad , \\
\beta_2 &:= 1/(R_{\perp\parallel})^2 \quad , \\
\beta_{32} &:= \frac{\frac{1}{R^t_\perp} - \frac{1}{R^c_\perp} - \frac{\alpha_1}{4}(R^t_\perp - R^c_\perp)}{R^t_\perp - R^c_\perp} \quad , \\
\beta_3 &:= \frac{1}{R^t_\perp} - \frac{\beta_1}{4} R^t_\perp - \beta_{32}\, R^t_\perp \quad .
\end{aligned} \tag{38}$$

If the inter-fiber failure criterion is achieved, stiffness degradation is initiated and controlled by a scalar damage variable d_{iff}. In contrast to the fiber failure criterion, the damage variable d_{iff} does not effect the stresses in fiber direction, see eq. (39). There is a remaining load carrying capacity in fiber direction, whereas in shear stress states or loadings perpendicular to the fiber direction the material has already failed. This is a reasonable assumption for long fiber reinforced composites, where in plane cracks cause a loss in stiffness perpendicular to the fibers, but further loadings in fiber direction can be applied:

$$\boldsymbol{\sigma}_{dam} = (1 - d_{iff})\,(\boldsymbol{\sigma}_{eff} - \mathbf{a}^T \boldsymbol{\sigma}_{eff} \mathbf{a}) \quad . \tag{39}$$

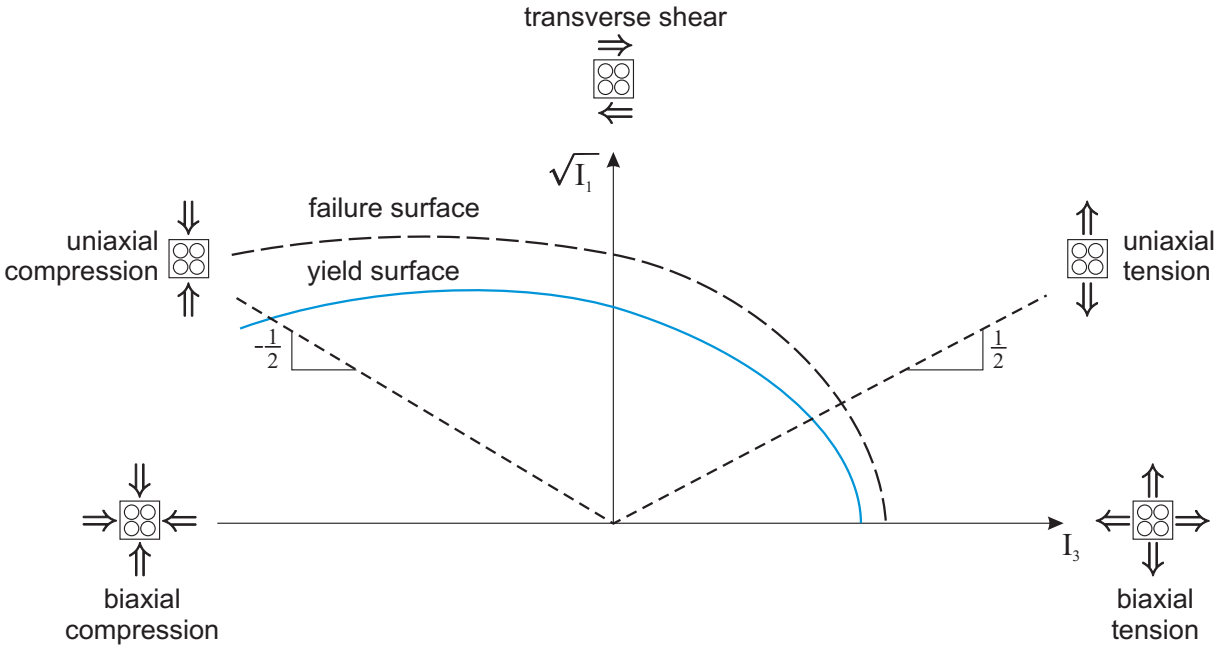

Figure 1: Yield and failure surface of the transversely isotropic material model in $\sqrt{I_1}$-I_3-invariant-plane

2.5.3 Fracture Energy Concept

Softening material behavior, which results macroscopically in a loss of material stiffness with adjacent failure, is preceded by the initiation and accumulation of microscopical defects such as cracks, micro-pores, shear-bands or crazes [9]. The initiation and accumulation of such defects are a matter of local defects and are restricted to a local zone, whose size depends on the material. So the width of the localizing zone, in which shear-bands or crazes develop, is a material constant [18]. When material damage occurs, the stress-strain relationship no longer represents the material's behavior accurately. Continuing to use the stress-strain relation introduces a strong mesh dependency based on strain localization, such that the energy dissipated decreases as the mesh is refined. HILLERBORG's fracture energy proposal [18] is used to reduce mesh dependency by creating a stress-displacement response after damage is initiated. Using brittle fracture concepts, HILLERBORG defines the energy G_f required to open a unit area of crack as a material parameter. The introduction of a characteristic internal length L_i, which is a measurement of the size of the localized area, the softening response after damage initiation is characterized by a stress-displacement response rather than a stress-strain response. The energy G_f required to open a unit area of crack, is

$$G_f = \int_{\bar{\varepsilon}^{pl}_{fail}}^{\bar{\varepsilon}^{pl}_{ult}} L_i \sigma_y d\bar{\varepsilon}^{pl} = \int_{\bar{u}^{pl}_{fail}}^{\bar{u}^{pl}_{ult}} \sigma_y d\bar{u}^{pl} \quad . \tag{40}$$

The implementation of this stress-displacement concept in a finite element model requires the definition of a characteristic element edge length L_e associated with an integration point. The fracture energy is then given as

$$G_f = \int_{\bar{\varepsilon}^{pl}_{fail}}^{\bar{\varepsilon}^{pl}_{ult}} L_e \sigma_y d\bar{\varepsilon}^{pl} = \int_{\bar{u}^{pl}_{fail}}^{\bar{u}^{pl}_{ult}} \sigma_y d\bar{u}^{pl} \quad . \tag{41}$$

This expression introduces the definition of the equivalent plastic displacement $\bar{u}_p$ as the fracture work conjugate of the yield stress σ_y after the onset of damage:

$$\bar{u}_p = L_e \bar{\varepsilon}_p \quad . \tag{42}$$

The definition of the characteristic length is based on the element geometry. For solid elements the cube root of the element volume is used. This definition of the characteristic length is chosen because the direction, in which fracture occurs, is not known in advance. Therefore, elements with large aspect ratios will have rather different behavior depending on the direction in which the crack evolves. This may lead to a mesh sensitivity of simulation results. In order to consider this mesh dependency, elements with an aspect ratio near unity should be used.
The introduction of the characteristic element edge length L_e means, that occurring localized strains are "smeared" or distributed over the particular element width.

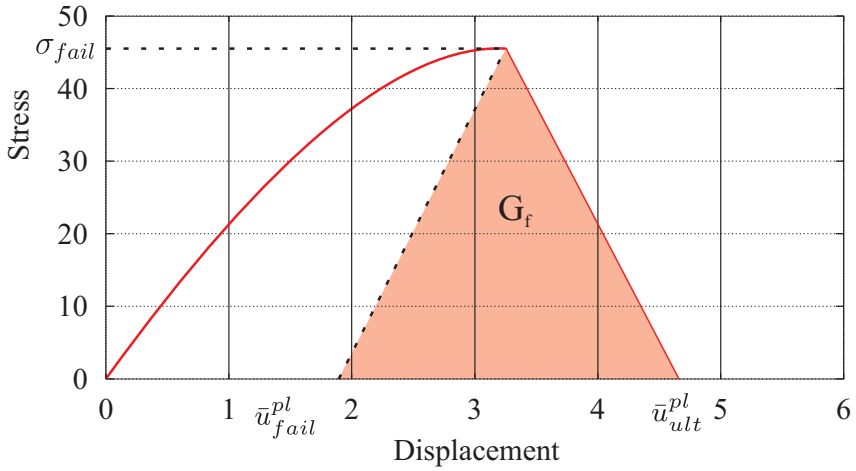

Figure 2: Fracture energy G_f, required to open a unit area of crack

2.6 Numerical Treatment

The present model has been implemented as a user-defined material into LS-DYNA [6], see also [7] and [11] for an overview of existing isotropic models for polymers in LS-DYNA. For time integration of the constitutive equations, a classical elastic-predictor plastic-corrector scheme is applied, see [13, 14, 15, 16]. Further, an associated flow rule is assumed. That is, the direction of plastic flow in stress space is given by the derivation of the yield function with respect to the stresses.

2.6.1 Projection Algorithm

Starting from the additive decomposition of the strain tensor and applying an associated flow rule, the trial stresses, assuming elastic behavior, are:

$$\begin{aligned} \boldsymbol{\sigma}^{tr}_{n+1} &= \mathbb{C}_e : \boldsymbol{\varepsilon}^{tr} \\ &= \boldsymbol{\sigma}_{n+1} + \gamma_{n+1}\mathbb{C}_e : \partial_{\boldsymbol{\sigma}} f \\ &= \boldsymbol{\sigma}_{n+1} + \gamma_{n+1}\mathbb{C}_e : [\mathbb{A} : \boldsymbol{\sigma} + \mathbf{B}] \\ &= [\mathbb{I} + \gamma_{n+1}\mathbb{C}_e : \mathbb{A}]\,\boldsymbol{\sigma}_{n+1} + \gamma_{n+1}\mathbb{C}_e : \mathbf{B} \quad . \end{aligned} \tag{43}$$

Conversion of eq. (43) gives the stresses at time $\boldsymbol{t}_{n+1}$:

$$\begin{aligned} \boldsymbol{\sigma}_{n+1} &= (\mathbb{I} + \gamma_{n+1}\mathbb{C}_e : \mathbb{A})^{-1} : (\boldsymbol{\sigma}^{tr} - \gamma_{n+1}\mathbb{C}_e : \mathbf{B}) \\ &= \mathbb{F}_{n+1} : (\boldsymbol{\sigma}^{tr}_{n+1} - \gamma_{n+1}\mathbb{C}_e\mathbf{B}) \end{aligned} \tag{44}$$

$$\text{with} \quad \mathbb{F} := [\mathbb{I} + \gamma_{n+1}\mathbb{C}_e : \mathbb{A}]^{-1} \quad . \tag{45}$$

Inserting eq. (45) into the active yield surface eq. (20) and enforcing the yield condition to be fulfilled at time t_{n+1}

$$f_{n+1} = \frac{1}{2}\boldsymbol{\sigma}_{n+1} : \mathbb{A} : \boldsymbol{\sigma}_{n+1} + \mathbf{B} : \boldsymbol{\sigma}_{n+1} - 1 = 0 \quad . \tag{46}$$

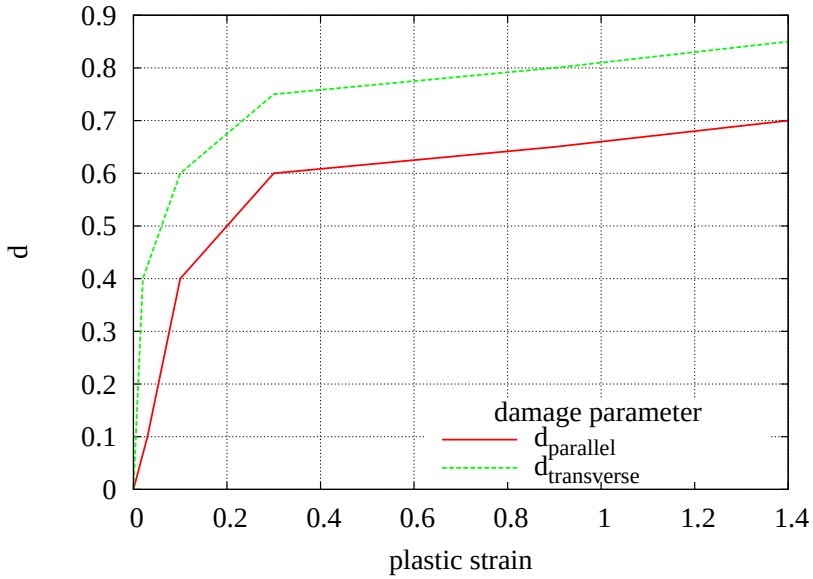

Figure 3: Input of damage parameters $d_{\parallel}$ and $d_{\perp}$ as tabulated data for fiber direction and transverse

leads to a nonlinear equation in γ_{n+1} which is solved by the NEWTON-RAPHSON method. With the root γ_{n+1} in hand, an update of the internal variables can be performed at the end of the current time step t_{n+1}:

$$\boldsymbol{\varepsilon}^{p}_{n+1} = \boldsymbol{\varepsilon}_{n} + \gamma_{n+1} \left(\mathbb{A} : \boldsymbol{\sigma} + \mathbf{B} \right) \quad . \tag{47}$$

As we refer to an explicit analysis, the consistent tangent modulus $\mathbb{C}_{ep}$ is not required.

3 Results

For testing the material model and illustrating the anisotropic behavior, material testings of Bayflex®180 with 22 per cent Tremin fill particles are simulated. The anisotropic characteristic of this material is due to the orientation of fibers which is in turn caused by the RRIM-process (reinforced reaction injection molding). The specimens are taken longitudinal and transverse to the preferred manufacturing conditioned direction. In order to get the local deformation behavior, the speckle-correlation technique is applied, see [10] for details of the required experimental setup. Basis of the determination of local strains is a two dimensional image recording. Thus, an isotropy concerning the lateral contraction is assumed. For transversely isotropic materials with loading parallel to the fiber direction it is a reasonable assumption. The isotropy of lateral contraction could be confirmed by additional material testings for quasi static loading ($10mm/s$ haul-off speed). Therefore, specimens taken both from the coign and the broadside are tested. The broadside is the surface of the plate, the coign is perpendicular to it. That is the specimens are rotated at 90 degrees around the tensile axis.

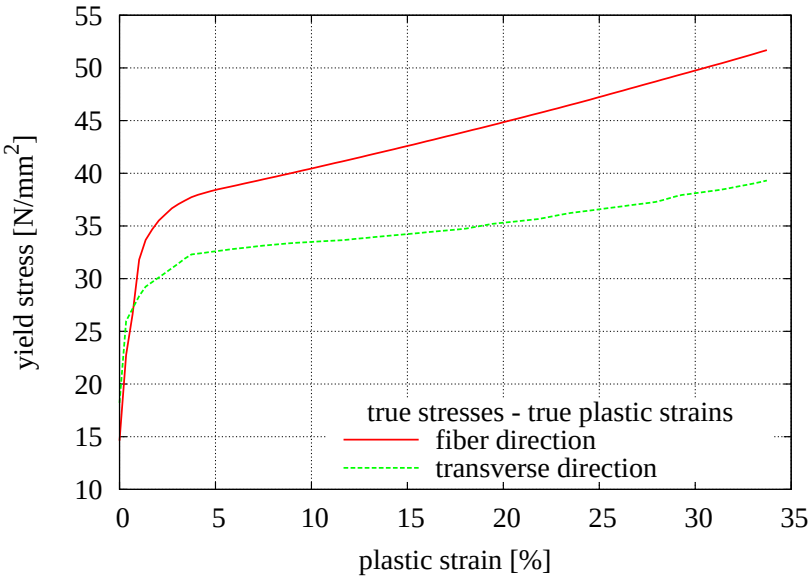

Figure 4: Experimentally obtained hardening curves, used as input data

3.1 Material Parameters

As only two uniaxial tensile tests longitudinal and transverse to fiber direction are performed with Bayflex®180, the yield surface parameters can't be determined completely according to our proposal of yield locus eq. (17). Therefore, the invariant I_3 is neglected. The parameter α_4 can be obtained directly from the uniaxial tensile test by using eq. (21). The parameter α_1 is determined by using the 4th material test in sec. 2.3.1 whereas the third invariant I_3 is neglected. Further it is assumed, that the transverse shear behavior, represented by the first invariant I_1 and the corresponding parameter α_1, is equal to the in-plane shear behavior, represented by I_2 and α_2. Thus, the yield locus used for Bayflex®180 is given by

$$f = \alpha_1 I_1 + \alpha_2 I_2 + \alpha_4 I_4^2 - 1 \quad . \tag{48}$$

As no unloading tests are performed with Bayflex®180, values for the damage variables $d_\perp$ and $d_\parallel$ are assumed. In order to illustrate the different unloading behavior in dependence of the fiber orientation, two different damage curves are input, see fig. 3. In order to demonstrate the regularizing effect of the fracture energy formulation, a strain energy release rate of $G_f = 0.168 \frac{N}{mm}$ is chosen.

3.2 Simulation Results

Fig. 5 shows the results of quasi-static loading for both the longitudinal and the transverse direction. The simulation results are in a quite good agreement with the experimentally obtained test data. As no unloading tests were performed with Bayflex®180, the damage

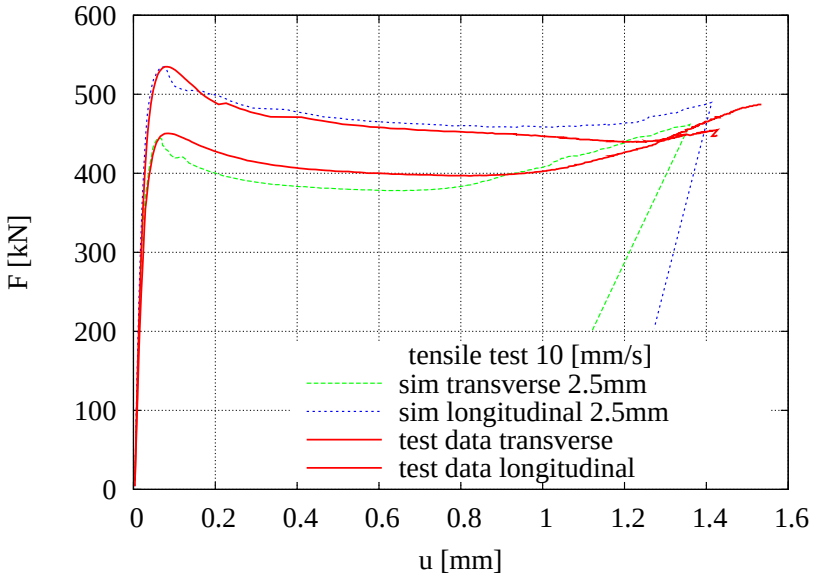

Figure 5: simulation results: unloading behavior

behavior of the material was assumed to be stronger developed in transverse direction. Therefore, two load curves are input, giving the transverse and longitudinal damage parameter over the corresponding plastic strains as described in sec. 2.4. The transversely isotropic damage behavior is reflected in the simulation results in different slopes of the unloading force-displacement curves for both directions, see fig. 5. The regularizing effect of the fracture energy concept according to HILLERBORG is shown in fig. 6. Therefore, simulations with different element sizes are performed. Both in the plastic region and in the post failure region the simulations are in a good agreement and no relevant mesh dependency can be observed after failure is initiated.

4 Summary and Outlook

A constitutive model for transversal isotropic material behavior has been proposed taking a C^1-continuous yield surface into account. A scalar damage formulation with an anisotropic damage evolution has been used for the approximation of the unloading behavior. Moreover, a very general failure surface that is affine to the yield surface has been added to the model for a triaxial-dependent prediction of fracture. The regularization has been realized by the consideration of an internal length. Tensile tests at Bayflex®180 has been simulated to show the applicability of the chosen model. The following features are topics of further investigation.

- strain rate effects : different strain rate sensitivity in preferred direction and transverse to preferred direction
- strain rate sensitivity of failure

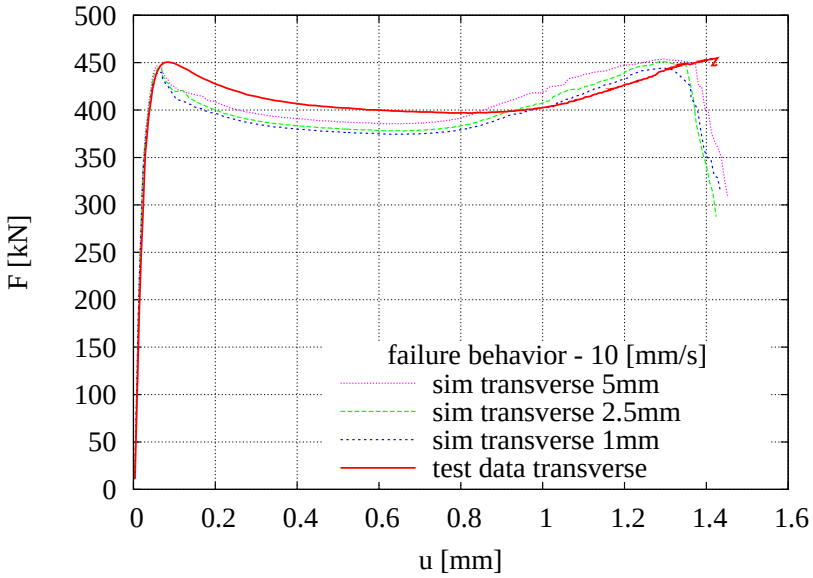

Figure 6: simulation results: failure

- accounting for different fracture energies in dependence of the failure mode and the direction
- introduction of a non-associated flow rule by use of a plastic potential in order to control dilatancy (and compression respectively) of volumetric plastic straining
- transition of the presented material model to the orthotropic case

Acknowledgements

The authors would like to express their sincere thanks to Dr. Sven Hobeika and Mr. Dirk Brüning from Bayer MaterialScience for providing the experimental data of Bayflex®180 and for fruitful discussions.

References

[1] S. Glaser, A. Wüst: Integrative Crash Simulation of Composite Structures - the Importance of Process Induced Material Data. Proceedings of the 4th LS-DYNA Forum, Bamberg, Germany, 2005.

[2] R. Krivachy: Modellierung und Simulation von extrudierten faserverstärkten Kunststoffen für dynamische Belastungen 4. Freiburg Workshop zum Werkstoff- und Strukturverhalten bei Crashvorgängen, crashMAT, 2006.

[3] M. Junginger: Charakterisierung und Modellierung unverstärkter thermoplastischer Kunststoffe zur numerischen Simulation von Crashvorgängen, Dissertation, Fraunhofer Institut für Kurzzeitsynamik, Heft Nr. 3, ISBN 3-8167-6339-1, 2004.

[4] S. Kolling, A. Haufe, M. Feucht and P.A. Du Bois: A semianalytical model for the simulation of polymers. *Proceedings of the 4th LS-DYNA Forum, Bamberg, Germany,* ISBN 3-86010-795-X, A-II:27–52, 2005.

[5] Boehler, J.P.: Applications of Tensor Functions in Solid Mechanics. CISM No. 292, Springer, 1987.

[6] J.O. Hallquist: LS-DYNA, Theoretical Manual, Livermore Software Technology Corporation, Report 1018, 1991.

[7] P.A. Du Bois: Crashworthiness Engineering Course Notes, Livermore Software Technology Corporation, 2004.

[8] P.A. Du Bois, S. Kolling, M. Koesters and T. Frank: Material behavior of polymers under impact loading. *International Journal of Impact Engineering*, 32(5):725–740, 2006.

[9] J. Lemaitre and J.-L. Chaboche: Mécanique des matériaux solides, Dunod, 1988.

[10] S. Hobeika: Lokales Deformationsverhalten bei hohen Geschwindigkeiten: Polymerphysik für die Crash-Simulation, Fachtagung Kunststoffe+Simulation 13.-14. Juni 2007, Fellbach/Stuttgart.

[11] F. Huberth, S. Hiermaier and M. Neumann: Material Models for Polymers under Crash Loads - Existing LS-DYNA Models and Perspective *Proceedings of the 4th LS-DYNA Forum, Bamberg, Germany,* ISBN 3-9809901-1-7, H-I-1-12, 2005.

[12] T. Frank, A. Kurz, M. Pitzer and M. Soellner: Development and validation of numerical pedestrian impactor models. 4th European LS-DYNA Users Conference, pp. C-II-01/18, 2003.

[13] J.C. Simo and T.J.-R. Hughes: Elastoplasticity and viscoplasticity - computational aspects. Springer Series in Applied Mathematics, Springer, Berlin, 1989.

[14] T.J.-R. Hughes: Numerical implementation of constitutive models: rate-independent deviatoric plasticity. In Nemat-Nasser et al: Theoretical foundation for large scale computations for nonlinear material behavior. Martinus Nijhoff Publishers, Dordrecht, 1984.

[15] T.J.-R. Hughes: Efficient and simple algorithms for the integration of general classes of inelastic constitutive equations including damage and rate effects. In T.J.-R. Hughes ,T. Belytschko: nonlinear finite element analysis course notes, 2003.

[16] P. Wriggers: Nichtlineare Finite-Element-Methoden, Springer-Verlag, 2001.

[17] Schröder, J.: Theoretische und algorithmische Konzepte zur phänomenologischen Beschreibung anisotropen Materialverhaltens. Dissertation, Universität Hannover (1995)

[18] A. Hillerborg, M. Modeer, and P. E. Petersson. Analysis of crack formation and crack growth in concrete by means of fracture mechanics and finite elements. *Cement and Concrete Research*, 6:773-782, 1976.

[19] Simo, J.C./ Hughes, T.J.R.: Computational Inelasticity. Interdisciplinary Applied Mathematics, Vol 7. Springer Verlag New York, 1998.

[20] Spencer, A.J.M.: Kinematic Constraints, Constitutive Equations and Failure Rules for Anisotropic Materials. In: Applications of Tensor Functions in Solid Mechanics, Ed.: Boehler,J.P., CISM No. 292, S. 187-201, Springer, 1987.

[21] Rogers, T.G.: Yield Criteria, Flow Rules and Hardening in Anisotropic Plasticity. In: Yielding, damage and failure of anisotropic solids, Ed.: Boehler, J.P. EGF Publication 5, 53-79, 1987.

[22] Eidel, B.: Anisotropic Inelasticity - Modelling, Simulation, Validation. Dissertation, Technische Universität Darmstadt, 2004.

